Draft version February 5, 2008
Preprint typeset using LaTeX style emulateapj v. 10/09/06

RAPID X-RAY DECLINES AND PLATEAUS IN SWIFT GRB LIGHT CURVES EXPLAINED BY A HIGHLY RADIATIVE BLAST WAVE

Charles D. Dermer
E. O. Hulburt Center for Space Research, Code 7653 Naval Research Laboratory, Washington, D.C. 20375-5352
Draft version February 5, 2008

ABSTRACT

GRB X-ray light curves display rapid declines followed by a gradual steepening or plateau phase in $\gtrsim 30\%$ of GRBs in the Swift sample. Treating the standard relativistic blastwave model in a uniform circumburst medium, it is shown that if GRBs accelerate ultra-high energy cosmic rays through a Fermi mechanism, then the hadronic component can be rapidly depleted by means of photopion processes on time scales $\sim 10^2$ – 10^4 s after the GRB explosion. While discharging the hadronic energy in the form of ultra-high energy cosmic ray neutrals and escaping cosmic-ray ions, the blast wave goes through a strongly radiative phase, causing the steep declines observed with Swift. Following the discharge, the blast wave recovers its adiabatic behavior, forming the observed plateaus or slow declines. These effects are illustrated by calculations of model bolometric light curves. The results show that steep X-ray declines and plateau features occur when GRB sources take place in rather dense media, with $n \gtrsim 10^2$ cm^{-3} out to $\gtrsim 10^{17}$ cm.

Subject headings: gamma rays: bursts — stars: winds, outflows — nonthermal radiation physics — cosmic rays

1. INTRODUCTION

The Swift telescope is providing a new database of GRB light curves consisting of a BAT light curve in the 15 – 150 keV range followed, after slewing within ≈ 100 s, by a detailed 0.3 – 10 keV XRT X-ray light curve and UVOT monitoring (Gehrels et al. 2004). Extrapolating the BAT light curve to the XRT range gives ~ 1 keV X-ray light curves since the trigger. O'Brien et al. (2006) present a catalog of the combined 0.3 – 10 keV light curves of 40 GRBs, of which 14 or so have measured redshifts, $\approx 30\%$ display rapid X-ray declines, and an additional $\approx 30\%$ display features unlike simple blast wave model predictions. In some GRBs, the 0.3 – 10 keV flux can decrease by 4 or 5 orders of magnitude over a period of $\lesssim 10^2$ seconds within several minutes after the GRB trigger (e.g., GRB 050915B, GRB 050422, GRB 050819). About one-half the XRT sample shows X-ray flares or short timescale ($\Delta t/t \ll 1$) structure at $\gtrsim 10^3$ s after the GRB trigger, and in some cases out to $\gtrsim 10^5$ s (e.g., GRB 050904 at $z = 6.29$ and GRB 050730 at $z = 3.97$).

Following the rapid X-ray declines, a more gradual steepening commences in most XRT light curves, as in the cases of GRB 050219A or GRB 050607. In several GRBs, e.g., GRB050315 or GRB050822, a plateau phase with rising and decaying features within 0.1 – 1 day after the GRB trigger are observed; this phase may also be found in other GRBs (GRB 050724 or GRB 050819), but could be contaminated or mimicked by a late-time X-ray flare. In a few GRBs (e.g., GRB 050401, GRB 050717), the X-ray decline is gentle and monotonic, but in general the XRT light curves, whether displaying overall convexity or concavity, reveal temporal structure and, oftentimes, X-ray flares (e.g., GRB 050712, GRB 050716, GRB 050726). A phenomenological model with two distinct components can fit the rapid decays and hardenings (Willingale et al. 2006), but lacks a physical basis. An acceptable physical model for GRB afterglows must be able to explain this diversity of behaviors.

A combined leptonic-hadronic GRB model is proposed in this paper as the cause of the rapid X-ray declines and plateaus discovered with Swift. The analysis presented here follows the standard blastwave model (e.g., Mészáros 2006). We show that if GRBs accelerate cosmic rays to ultra-high energies, then for certain classes of GRBs, the blastwave will become strongly radiative during the early afterglow, and consequently will exhibit rapid X-ray declines. This class of GRBs is defined by a range of blast wave and environmental parameters. One set of parameters that produces such declines has initial Lorentz factors $\Gamma_0 \sim 100$ – 300, apparent total energy releases $\gtrsim 10^{54}$ ergs (and absolute energy releases $\lesssim 10^{52}$ ergs), and surrounding medium density $n \gtrsim 10^2$ cm^{-3}, which is assumed to be proton dominated. The blast wave microphysical parameters ϵ_e, ϵ_B must both be $\gtrsim 0.1$.

For these GRBs, Fermi processes in the blast wave are assumed to accelerate proton and ions, like they do electrons, to ultrarelativistic energies. By making reasonable approximations for the acceleration rate as a fraction of the Larmor rate, and particle escape through Bohm diffusion, we find that photohadronic losses and particle escape significantly deplete the internal energy of the blast wave, causing the blast wave dynamics to be strongly affected. Photopion interactions by the ultrarelativistic protons and secondary neutrons with the internal synchrotron photons make a source of escaping neutrons, neutrinos and cascade γ rays, in addition to a generally weaker proton synchrotron component.

In Section 2, a standard blast-wave physics analysis for emissions from a GRB external shock in the prompt and early afterglow phase is presented, and timescales for the various processes are calculated for an adiabatic blast wave that decelerates by sweeping up material from

Electronic address: dermer@gamma.nrl.navy.mil

a uniform surrounding medium. Parameter sets that allow a large fraction of the internal energy to be radiatively discharged through hadronic processes are graphically examined in Section 3. In Section 4, the equations for blastwave evolution are solved in the case of internal energy that is promptly radiated or is exponentially depleted with time. Synthetic bolometric light curves are calculated. Although these cannot be directly compared to the Swift X-ray light curves without taking into account spectral effects and more complicated radiation physics, the bolometric light curves exhibit many of the features observed with Swift.

Discussion of multiwavelength and multichannel γ-ray, cosmic-ray, and neutrino predictions for this model is found in Section 5, including a comparison with other models for the X-ray declines. The study is summarized in Section 6.

2. ANALYSIS

The energy flux $\Phi_E = dE/dAdt = \nu F_\nu = f_\epsilon = L_*/4\pi d_L^2$, where $d_L = 10^{28} d_{28}$ cm is the luminosity distance, the source luminosity $L_* = 4\pi x^2 c u'_0 \Gamma^2$, x is the distance of the blast wave from the explosion center, and $\Gamma = \Gamma(x)$ is the blast wave Lorentz factor at x. The measured dimensionless photon energy $\epsilon \equiv h\nu/m_e c^2$ is related to the emitted photon energy ϵ' through the relation $\epsilon' \cong (1+z)\epsilon/2\Gamma$, and the differential distance traveled by the blast wave during reception time dt is $dx \cong 2\Gamma^2 cdt/(1+z)$, where z is the source redshift, and primes denote quantities in the comoving fluid frame. Thus the comoving energy density

$$u'_{\epsilon'} = m_e c^2 \epsilon'^2 n'_{ph}(\epsilon') \cong \ k_{kin}\ \frac{d_L^2 f_\epsilon}{cx^2\Gamma^2}\ , \qquad (1)$$

where $k_{kin} \approx 1/3$ gives the photon energy density that produces a received spectrum with peak νF_ν flux $= f_\epsilon$ (Dermer 2004). Relating x to the measured variability time gives the proper spectral density of the radiating fluid as a function of the Doppler factor. The GRB spectrum is approximated by the broken power-law form

$$n'_{ph}(\epsilon') = \frac{k_{kin} d_L^2 f_{\epsilon_{pk}}}{cx^2\Gamma^2 m_e c^2}\ \frac{[u^a H(1-u) + u^b H(u-1)]}{\epsilon'^{\ 2}}\ , \quad (2)$$

where $u = \epsilon/\epsilon_{pk} = \epsilon'/\epsilon'_{pk}$, $f_{\epsilon_{pk}} = 10^{-6} f_{-6}$ ergs cm^{-2} s^{-1} is the peak νF_ν flux at the νF_ν peak photon energy ϵ_{pk}, $a > 0$ and $b < 0$ are the νF_ν indices, and the Heaviside function $H(y) = 1$ for $y \geq 1$ and $H(y) = 0$ otherwise restricts the lower and upper branches of the spectrum to their respective ranges.

2.1. *Adiabatic Blast Wave*

Consider a blast wave with coasting Lorentz factor $\Gamma_{300} = \Gamma_0/300$ and apparent *total* isotropic energy release $E_0 = 10^{54} E_{54}$ ergs, so that its absolute energy release, due to collimation of the relativistic outflows, is $\lesssim 10^{52}$ ergs. If the blast wave sweeps through a uniform surrounding medium with proton density $n_0 = 100 n_2$ cm^{-3}, it will slow down on the deceleration length scale

$$x_d = \frac{3E_0}{4\pi m_p c^2 n_0 \Gamma_0^2} \cong 2.6\times 10^{16} \big(\frac{E_{54}}{n_2 \Gamma_{300}^2}\big)^{1/3}\ \text{cm} \qquad (3)$$

(Mészáros & Rees 1993). A relativistic adiabatic blast wave decelerates according to the relation

$$\Gamma = \Gamma_0/\sqrt{1 + 2(x/x_d)^3} \qquad (4)$$

(Böttcher & Dermer 2000), from which can be derived the asymptotes

$$\frac{x}{x_d} = \begin{cases} \tau, & \tau \ll 1 \\ (2\tau)^{1/4}, & \tau \gg 1 \end{cases} \qquad (5)$$

and

$$\frac{\Gamma}{\Gamma_0} = \begin{cases} 1, & \tau \ll 1 \\ 2^{-7/8}\tau^{-3/8}, & \tau \gg 1 \end{cases} . \qquad (6)$$

Here the dimensionless time $\tau \equiv t/t_d = t'/t'_d$, where the deceleration timescale is

$$t_d = \frac{(1+z)x_d}{\Gamma_0^2 c} \cong 9.6(1+z)\big(\frac{E_{54}}{n_2\Gamma_{300}^8}\big)^{1/3}\ \text{s}\ , \qquad (7)$$

and the inverse of the comoving deceleration timescale is

$$t'^{-1}_d = (\frac{x_d}{\Gamma_0 c})^{-1} \cong 3.5\times 10^{-4}\big(\frac{n_2\Gamma_{300}^5}{E_{54}}\big)^{1/3}\ \text{s}^{-1}\ . \qquad (8)$$

The available time in the comoving frame is

$$t'_{ava} = t'_d \begin{cases} \tau, & \tau \ll 1 \\ (2^{17/8}/5)\tau^{5/8} \cong 0.872\tau^{5/8}, & \tau \gg 1 \end{cases} , \qquad (9)$$

2.2. *Blast Wave Physics*

We treat the photopion process in the fast cooling regime (Sari et al. 1998). The minimum Lorentz factor $\gamma_{min} = \epsilon_e \mathcal{F}_p m_p \Gamma/m_e$, where $\mathcal{F}_p = (p-2)/(p-1)$ and $2 < p < 3$. The emission detected by Swift is assumed to be predominately nonthermal synchrotron radiation. The mean magnetic field in the fluid frame is $B = bB_{cr} = \sqrt{32\pi m_p c^2 n_0 \epsilon_B}\Gamma \cong 0.4\sqrt{\epsilon_B n_0}\ \Gamma$ G $\cong 370\sqrt{\epsilon_{B-1} n_2}\ \Gamma_{300}(\Gamma/\Gamma_0)$ G, where $B_{cr} = m_e^2 c^3/e\hbar \cong 4.414\times 10^{13}$ G, and the minimum mean observed synchrotron photon energy from electrons with γ_{min} is

$$\epsilon_{min} \cong \frac{\Gamma b \gamma_{min}^2}{1+z} \cong \frac{0.85\sqrt{\epsilon_{B-1} n_2}\epsilon_{e-1}^2 \mathcal{F}_{5/2}^2 \Gamma_{300}^4 (\Gamma/\Gamma_0)^4}{1+z}\ . \qquad (10)$$

The cooling Lorentz factor $\gamma_c = 3m_e(1+z)/16 m_p \sigma_{\rm T} \epsilon_B n_0 \Gamma^3 c t_d \tau$, and the dimensionless cooling frequency (in units of $m_e c^2$) is given by

$$\epsilon_c \cong \frac{2.3\times 10^5 (1+z)}{(\epsilon_B n_0)^{3/2}\Gamma^4 t_d^2 \tau^2}\ \cong\ \frac{1.0\times 10^{-8}\Gamma_{300}^{4/3}(\Gamma/\Gamma_0)^{-4}}{\epsilon_{B-1}^{3/2} n_2^{5/6}(1+z)E_{54}^{2/3}\tau^2}\ . \qquad (11)$$

Comparing eqs. (10) and (11) shows that we are in the strong cooling regime, $\epsilon_c < \epsilon_{min}$, when

$$\tau \lesssim 7\times 10^5\ (\epsilon_{e-1}\epsilon_{B-1}\mathcal{F}_{5/2})^2 n_2^{4/3} E_{54}^{2/3} \Gamma_{300}^{8/3}\ . \qquad (12)$$

The photon energy at the peak of the νF_ν synchrotron spectrum for the fast-cooling blast wave is given by

$$\epsilon_{pk} \cong\ \frac{0.85\sqrt{\epsilon_{B-1} n_2}\epsilon_{e-1}^2 \mathcal{F}_{5/2}\Gamma_{300}^4}{1+z} \begin{cases} 1, & \tau \ll 1 \\ 0.09\tau^{-3/2}, & \tau \gg 1 \end{cases} , \qquad (13)$$

and the νF_ν peak flux is given by

$$f_{\epsilon_{pk}} \cong \frac{\Gamma^2}{4\pi d_L^2}\ (\frac{4}{3} c\sigma_{\rm T} U_B)\ \gamma_{min}^3 N'_e(\gamma_{min}; x)\ . \qquad (14)$$

In this expression, $U_B = B^2/8\pi$ is the magnetic-field energy density in the comoving frame. For the fast-cooling regime, $N'_e(\gamma_{min}) \cong N_e(x)\gamma_c\gamma_{min}^{-2}$, and $N_e(x) = 4\pi n_0 x^3/3$. Thus

$$f_{\epsilon_{pk}}(10^{-6}\ \mathrm{ergs\ cm^{-2}\ s^{-1}}) \cong$$
$$2.7\ \frac{\epsilon_{e-1}\mathcal{F}_{5/2}n_2^{1/3}E_{54}^{2/3}\Gamma_{300}^{8/3}}{d_{28}^2}\begin{cases}\tau^2, & \tau \lesssim 1\\ (2\tau)^{-1}, & \tau \gg 1\end{cases}. \quad (15)$$

2.3. *Photopion Losses*

The energy-loss rate due to photopion production on the GRB synchrotron radiation field is

$$r_{\phi\pi} = t'^{-1}_{\phi\pi}(\gamma'_p) \cong \frac{c}{2\gamma'^2_p}\int_0^\infty d\epsilon'\ \frac{n'_{ph}(\epsilon')}{\epsilon'^2}\times$$
$$\int_0^{2\gamma'_p\epsilon'} d\epsilon'_r\ \epsilon'_r\sigma^K_{\phi\pi}(\epsilon'_r) \approx \frac{k_{kin}\hat{\sigma}d_L^2 f_{\epsilon_{pk}}}{x^2\Gamma^2 m_e c^2\epsilon_{pk}}\times$$
$$\{H(1-y)\big[\frac{y^2}{3-a} - \frac{2y^{a-1}}{(3-a)(a-1)} + \frac{1}{a-1}\big]$$
$$+\ \big[\frac{\max(1,y)^{b-1}}{1-b} - \frac{y^2\max(1,y)^{b-3}}{3-b}\big]\}\,, \quad (16)$$

after substituting eq. (2) into eq. (16), with $y \equiv \epsilon'_{thr}/2\gamma'_p\epsilon'_{pk}$. Here we use the approximation of Atoyan & Dermer (2003), where the product of the photopion cross section and inelasticity is $\sigma^K_{\phi\pi}(\epsilon'_r) = \hat{\sigma} \cong 70\ \mu\mathrm{b}\ H(\epsilon'_r - \epsilon'_{thr})$, and the threshold dimensionless photon energy for photopion production is $\epsilon'_{thr} \cong 400$ (i.e., $m_e c^2\epsilon'_{thr} \approx 200$ MeV).

The asymptotes of eq. (16) are

$$t'^{-1}_{\phi\pi}(\gamma_p) \cong K_{\phi\pi}(\bar{\gamma}_p)\begin{cases} y^{b-1}, & y \geq 1\\ \frac{(3-b)(a-b)}{2(a-1)}\,, & y \ll 1,\ 1 \leq a \leq 3\\ \frac{(1-b)(3-b)}{(3-a)(1-a)}\ y^{a-1}, & y \ll 1,\ 0 \leq a \leq 1\end{cases} \quad (17)$$

where $y = 1$ defines the Lorentz factor $\bar{\gamma}'_p$ of protons that interact primarily with internal synchrotron photons at the νF_ν peak frequency ϵ'_{pk}. We call $\bar{E}_p = m_p c^2\bar{\gamma}_p = m_p c^2\Gamma\bar{\gamma}'_p$ the *peak cosmic-ray proton energy*, as it is the characteristic energy of protons with Lorentz factor $\bar{\gamma}'_p$ that would escape from the blast wave with Lorentz $\bar{\gamma}_p$ factor as measured by a local observer. Hence the peak cosmic-ray proton energy is

$$\bar{E}_p = \frac{m_p c^2\Gamma^2\epsilon'_{thr}}{(1+z)\epsilon'_{pk}} \cong \frac{1.7\times10^{16}(\Gamma/300)^2}{(\frac{1+z}{2})\epsilon_{pk}}\ \mathrm{eV}\,, \quad (18)$$

and

$$K_{\phi\pi}(\bar{\gamma}_p) = \frac{2k_{kin}\hat{\sigma}d_L^2 f_{\epsilon_{pk}}}{x^2\Gamma^2 m_e c^2\epsilon'_{pk}(1-b)(3-b)} \cong$$
$$\frac{1.1\times10^{-6}k_{kin}d_{28}^2 f_{-6}}{(1-b)(3-b)(1+z)x_{16}^2(\Gamma/300)\epsilon_{pk}}\ \mathrm{s^{-1}}\,, \quad (19)$$

where $x = 10^{16}x_{16}$ cm.

2.4. *Rates and Limits for Ultrarelativistic Protons*

2.4.1. *Adiabatic Loss Rate*

Adiabatic expansion losses operate on the same timescale as the available time, so for comparison of the adiabatic loss rate to other rates, we write $t'^{-1}_{adi} \cong t'^{-1}_{ava}$, using eq. (9).

2.4.2. *Photopion Loss Rate*

Substituting eqs. (5), (6), and (13) into eq. (17) gives the comoving photopion energy-loss rate

$$t'^{-1}_{\phi\pi}(\bar{E}_p) \cong \frac{5.2\times10^{-7}k_{kin}n_2^{1/2}\ \mathrm{s^{-1}}}{(1-b)(3-b)\Gamma_{300}^2\epsilon_{B-1}^{1/2}\epsilon_{e-1}}\begin{cases}1, & \tau \lesssim 1\\ 2^{23/8}\tau^{3/8}, & \tau \gg 1\end{cases} \quad (20)$$

at the characteristic energy

$$\bar{E}_p(\mathrm{eV}) \cong \frac{4\times10^{16}}{\sqrt{\epsilon_{B-1}n_2}\epsilon_{e-1}^2\mathcal{F}_{5/2}\Gamma_{300}^2}\begin{cases}1, & \tau \lesssim 1\\ 3.4\tau^{3/4}, & \tau \gg 1\end{cases} \quad (21)$$

of an escaping cosmic ray, as measured by a stationary observer in the local source frame.

2.4.3. *Acceleration Rate*

Because a significant energy gain by a particle can take place through Fermi acceleration mechanisms on times not shorter than the Larmor time $t'_{\rm L} = mc^2\gamma'_p/eBc = (mc/eB)(\gamma/\Gamma)$ (Rachen & Mészáros 1998), the acceleration rate in the proper frame can be written as $r_{acc} = t'^{-1}_{acc} = \zeta_{acc}t'^{-1}_{\rm L}$, with the acceleration parameter $\zeta_{acc} \lesssim 1$. Hence the acceleration rate at the peak cosmic-ray proton energy $\bar{E}_p$ is given by

$$r_{acc}(\bar{E}_p) \cong$$
$$25\zeta_{acc}\ n_2\epsilon_{B-1}\Gamma_{300}^4\epsilon_{e-1}^2\mathcal{F}_{5/2}\ \mathrm{s^{-1}}\begin{cases}1, & \tau \lesssim 1\\ \frac{1}{11.4\tau^{3/2}}, & \tau \gg 1\end{cases} \quad (22)$$

The acceleration rate for $10^{20}E_{20}$ eV cosmic ray protons is

$$r_{acc}(E_{20}) \cong$$
$$\frac{1.1\times10^{-3}(\zeta_{acc}/0.1)\sqrt{\epsilon_{B-1}n_2}}{E_{20}}\frac{\Gamma_{300}^2}{(1+2^{7/8}\tau^{3/8})^2}\ \ \mathrm{s^{-1}}\,. \quad (23)$$

Here we consider a standard acceleration parameter $\zeta_{acc} \cong 0.1$. Values of $\zeta_{acc} \cong 1$ require unreasonably efficient particle acceleration, with particles gaining a large fraction of their energy in a single Larmor timescale. If $\zeta_{acc} \ll 0.1$, then GRBs would not accelerate cosmic rays sufficiently rapidly to make ultra-high energy cosmic rays.

2.4.4. *Escape Rate*

The mean escape rate using the Bohm diffusion approximation is given by $t'_{esc} = \langle x\rangle^2/2\kappa_{\rm B}$, where $\kappa_{\rm B} = c^2 t'_{\rm L}/3$ is the diffusion coefficient. For particle acceleration in GRB blast waves, the characteristic dimension $\langle x\rangle$ is the shell width $\Delta' = f_\Delta x/\Gamma$, and $f_\Delta \cong 1/12$ for the width of the shocked fluid shell swept up from the circumburst medium by an adiabatic relativistic blast

waves (e.g., Panaitescu & Mészáros 1999). Thus the escape rate is

$$t'^{-1}_{esc} \cong \frac{2cE_p\Gamma\zeta_{esc}}{3eBf_\Delta^2 x_d^2}\ \frac{1}{(x/x_d)^2}\ , \qquad (24)$$

where ζ_{esc} is a parameter that allows particle escape on timescales shorter ($\zeta_{esc} > 1$) or longer ($\zeta_{esc} < 1$) than the escape timescale set by Bohm diffusion. If the GRB blast-wave shell entrains a randomly oriented, tangled magnetic field, then depending on the coherence length of the disordered magnetic field, the particles could diffuse more rapidly than given by Bohm diffusion, so that $\zeta_{esc} \gtrsim 1$. In contrast, if the GRB blast wave is assumed to entrain an ordered field, for example, a toroidal geometry in a jetted fireball, then escape could be impeded compared to the Bohm timescale, so that $\zeta_{esc} \ll 1$. Here we consider the Bohm limit for the rate at which particles escape, keeping in mind that the actual escape rate could be quite different.

The escape rate for protons with characteristic energy $\bar{E}_p$, eq. (21), is

$$t'^{-1}_{esc}(\bar{E}_p) \cong \frac{5\times10^{-7}\zeta_{esc}\ \mathrm{s}^{-1}}{\epsilon_{B-1}n_2^{1/3}\epsilon_{e-1}^2\mathcal{F}_{5/2}\Gamma_{300}^{2/3}} \begin{cases} \tau^{-2}, & \tau \lesssim 1 \\ 2.4\tau^{1/4}, & \tau \gg 1 \end{cases} . \qquad (25)$$

The escape rate for $10^{20}E_{20}$ eV cosmic ray protons is

$$t'^{-1}_{esc}(E_{20}) \cong \frac{1\times10^{-3}E_{20}n_2^{1/6}\Gamma_{300}^{4/3}\zeta_{esc}\ \mathrm{s}^{-1}}{\sqrt{\epsilon_{B-1}}E_{54}^{2/3}} \begin{cases} \tau^{-2}, & \tau \lesssim 1 \\ (2\tau)^{-1/2}, & \tau \gg 1 \end{cases} . \qquad (26)$$

2.4.5. *Size Scale Limitation*

We also have the Hillas (1984) condition that the Larmor radius be smaller than the characteristic size scale of the system, which is the shell width Δ'. Requiring $r_{\rm L} = (mc^2/eB)(\gamma/\Gamma) \lesssim \Delta' \cong f_\Delta x/\Gamma$ implies a limit to maximum proton energy, given by

$$E_p^{\rm H}(10^{20}\ \mathrm{eV}) = 2.4\,\epsilon_{B-1}^{1/2}n_2^{1/6}\Gamma_{300}^{1/3}E_{54}^{1/3} \begin{cases} \tau, & \tau \lesssim 1 \\ \frac{\tau^{-1/8}}{2^{5/8}}, & \tau \gg 1 \end{cases} , \qquad (27)$$

using the asymptotes, eqs. (5) and (6). Note the slow late-time decline $E_p^{\rm H} \propto t^{-1/8}$ when $\tau \gg 1$ (Vietri 1998; Böttcher & Dermer 1998). Thus we see that standard parameter values allow Fermi acceleration of protons to ultra-high energies in GRB blast waves when $\zeta_{acc} \gtrsim 0.1$ and $\zeta_{esc} \cong 1$, making GRBs a viable candidate for UHECR production.

2.4.6. *Proton Synchrotron Energy Loss Rate*

The inverse of the synchrotron energy-loss timescale for an escaping proton with Lorentz factor $\gamma_p = \Gamma\gamma'_p$ is

$$r_{p,syn} = t'^{-1}_{p,syn}(\gamma_p) = |\frac{\dot{\gamma}'_{p,syn}}{\gamma'_p}| = \frac{16}{3}\,c\sigma_{\rm T}n_0\epsilon_B\Gamma\,(\frac{m_e}{m_p})^2\gamma_p$$

$$\cong 9.4\times10^{-6}n_2\epsilon_{B-1}\Gamma_{300}E_{20}\,(\frac{\Gamma}{300})\ \mathrm{s}^{-1}\ . \qquad (28)$$

The mean proton synchrotron photon energy, in units of m_ec^2, from protons with energies $10^{20}E_{20}$ eV ($E_{20} \cong$ $\gamma_{11} = \gamma_p/10^{11}$) as measured in the stationary frame, is given by

$$\epsilon_{p,syn} = \frac{3\Gamma}{1+z}\,\frac{B}{B_{cr}}\,\frac{m_e}{m_p}\,\gamma'^2_p \cong 4.5\times10^5\,\frac{\epsilon_{B-1}n_2E_{20}^2}{1+z}\ , \qquad (29)$$

independent of time in the relativistic deceleration phase—provided of course that ϵ_B is time-independent and $n_2 = const.$

TABLE 1
Parameter Sets Used in Analysis

	Stnd. Set	Set 1	Set 2
z	1	1	1
Γ_{300}	1	1	0.5
E_{54}[a]	1	1	10
n_2[b]	1	10	10
ϵ_{e-1}	1	3	1
ϵ_{B-1}	1	3	3
ζ_{acc}	0.1	0.1	0.1
ζ_{esc}	1	1	1
t_d(s)	19.3	8.9	122
$x_d(10^{16}$ cm)	2.6	1.2	4.1

[a] Apparent isotropic energy release in units of 10^{54} ergs.[b] Circumburst medium density, assumed uniform and dominated by H, in units of 100 cm^{-3}.

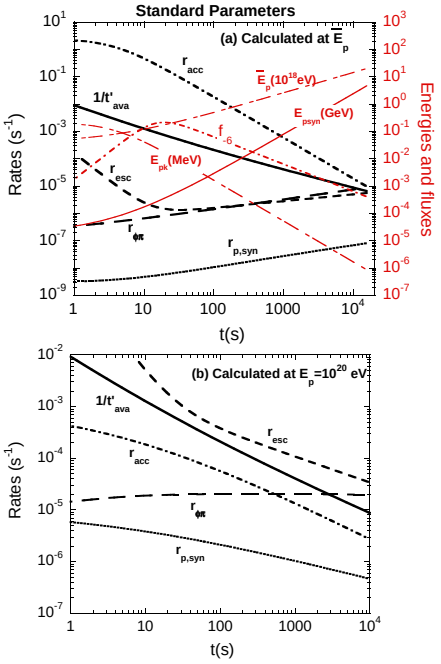

FIG. 1.— (a) Characteristic rates and energies calculated at $\bar{E}_p$, (b) characteristic rates calculated at $E_p = 10^{20}$ eV, using the Standard Parameter set.

3. RESULTS

For initial parameter estimation, we adopt the Standard Parameter Set given in Table 1, with $z = 1, \Gamma_{300} = 1, E_{54} = 1, n_2 = 1, \epsilon_{e-1} = 1$, and $\epsilon_{B-1} = 1$. This set is motivated by values that reproduce typical peak fluxes and durations for BATSE GRBs at $z \approx 1$ (Chiang & Dermer 1999), except that here $\epsilon_B = 0.1$ rather than $\epsilon_B \cong 10^{-4}$.

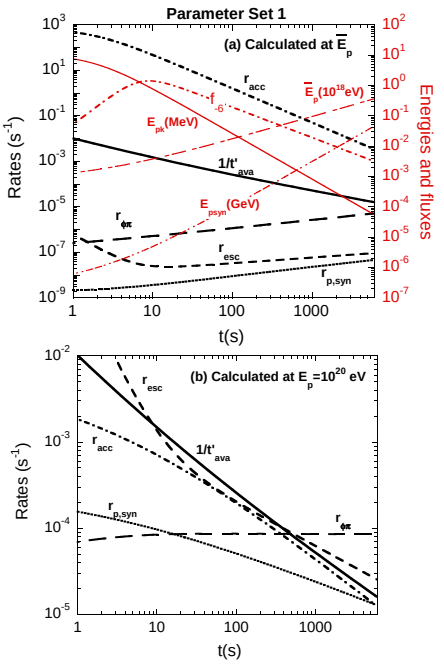

FIG. 2.— As in Fig. 1, but calculated for Parameter Set 1, with the energy of electrons, protons, and magnetic field in approximate equipartition.

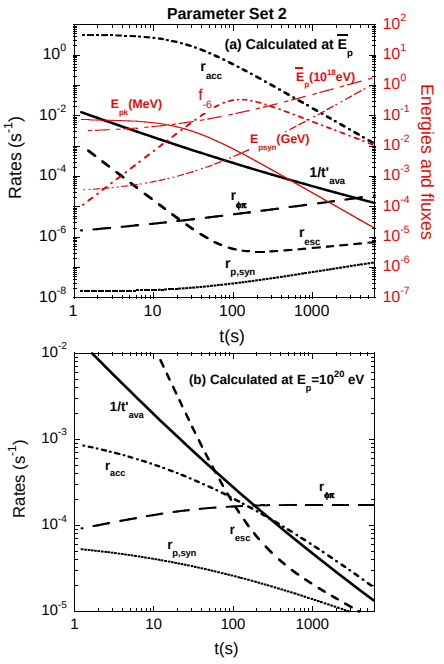

FIG. 3.— As in Fig. 1, but calculated for Parameter Set 2.

Fig. 1(a) shows the Standard Parameter rates of acceleration, photopion losses, proton synchrotron losses and escape for cosmic rays with energy $\bar{E}_p$, the νF_ν peak photon energy ϵ_{pk}, the cosmic-ray peak energy $\bar{E}_p$, and the mean proton synchrotron photon energy $E_{p,syn} = m_e c^2 \epsilon_{p,syn}$ radiated by protons with energy $\bar{E}_p$. Here and throughout we use an acceleration factor $\zeta_{acc} = 0.1$, an escape factor $\zeta_{esc} = 1$, and kinematic factor $k_{kin} = 1$.

From the top panel in Fig. 1, one sees that the acceleration rate exceeds the inverse of available time throughout the early afterglow phase, so cosmic rays with energies $\sim \bar{E}_p$ are in principle easily accelerated through Fermi processes to energies $\gtrsim \bar{E}_p$. Only at several hours into the afterglow do photopion losses limit acceleration to $E_p \lesssim \bar{E}_p$, which by then is $\gtrsim 10^{19}$ eV. At these late times, proton synchrotron emissions make a $\gtrsim$1% contribution to the total loss rate. The diffusive escape rate of protons can appear as a $\gtrsim$1% effect on the total rate, but is generally insignificant in the early afterglow. The external shock emission from this GRB is brightest ≈ 20 s after first being detected, though shell collisions could make brighter features during the prompt and afterglow phases (see Discussion).

The acceleration, escape, and loss rates for a cosmic ray proton with $E_p = 10^{20}$ eV are plotted in Fig. 1b. As can be seen, there isn't enough time to accelerate cosmic rays to $\gtrsim 10^{20}$ eV energies for these parameters, so there cannot be significant $\gtrsim 10^{20}$ eV (super-GZK) cosmic ray production or photopion losses from such GRBs (unless $\zeta_{acc} \gg 0.1$). Protons would also escape before a significant fraction could be accelerated to such energies.

A set of parameters that overcomes these limitations is easily found. Consider Parameter Set 1 in Table 1, with $z = 1, \Gamma_0 = 300, E_{54} = 1, n_2 = 10, \epsilon_{e-1} = 3, \epsilon_{B-1} = 3$, giving the rates, fluxes, and energies shown in Fig. 2. For 10^{20} eV cosmic rays shown in the lower panel, an interesting conjunction occurs when $r_{\phi\pi} \approx 1/t'_{ava} \lesssim r_{acc}$, which happens here at ≈ 300 s. Protons accelerated to $\approx 10^{20}$ eV energies are converted, $\sim 1/2$ of the time[1], to ultrarelativistic neutrons that escape from the blast wave to form one component of a neutral beam (Atoyan & Dermer 2003), in addition to neutrinos and γ rays.

The GRB formed in Parameter Set 1, Fig. 2, has a rather high $E_{pk} \sim 8$ MeV—which may be irrelevant in an internal/external scenario—but values of $\Gamma_0 \lesssim 300$ will lower ϵ_{pk} during the prompt phase and lengthen the prompt phase duration. Fig. 3 shows the results for Parameter Set 2 with $z = 1, \Gamma_0 = 150, E_0 = 10^{55}$ ergs, $n_2 = 10, \epsilon_{e-1} = 1, \epsilon_{B-1} = 3$. This GRB peaks $\gtrsim 50$ s after the trigger, has a lower ϵ_{pk}, and reaches a slightly lower $f_{\epsilon_{pk}}$ peak flux than in Fig. 2.

Parameter Sets 1 and 2 model fast-cooling GRBs with $\epsilon_e = 0.3$ and $\epsilon_e = 0.1$, respectively, that exhibit a radiative photopion phase. By letting ϵ_e= 30% for Set 1, it is understood that a large fraction of the swept-up power is found in nonthermal electrons rather than in baryons or fields. A large body of parameter values clustering around the Parameter Set 1 values predict strong photopion losses in the early afterglow phase, especially if $\zeta_{acc} \gtrsim 0.1$ is allowed. If $\epsilon_e \lesssim 0.1$ is assumed, as in Parameter Set 2, then agreement with GRB energetics for GRBs with *apparent bolometric γ-ray energy* $\gtrsim 10^{54}$ ergs, which represents a significant fraction of pre-Swift GRBs (Friedman & Bloom 2005), means that a large fraction of GRBs also have *apparent total energy* $E_{54} \gtrsim 10$, due to the unknown efficiency of converting the total energy into γ rays. Even for small ϵ_e models,the necessary large values of total apparent total energy can result in strong

[1] The charge-changing fraction is not 1/3, as expected for Δ resonance excitation and decay, due to the inclusion of direct pion channels above threshold, and multi-pion production at energies far above threshold.

photopion losses. Thus if GRBs accelerate UHECRs, then photohadronic losses efficiently deplete GRB internal energy and affect the blastwave dynamics over a wide range of GRB parameters.

4. BLAST WAVE EVOLUTION WITH RADIATIVE DISCHARGE

The previous section showed that with reasonable parameter values, photopion production and escape can rapidly deplete internal blastwave energy in the early afterglow when hadronic processes become important. We now calculate model light curves resulting from the radiative discharge of internal energy through photohadronic processes. The dynamics of the blast wave is numerically solving using the equation of relativistic blastwave evolution, including adiabatic losses, given by

$$-\frac{dP/dx}{\Gamma^2-1} = \frac{\Gamma P\,\frac{dm}{dx} + \left(\frac{\Gamma^2}{P}\right)\frac{dU'_{adi}}{dx}}{M_0 + m(x) + U'} \tag{30}$$

(Dermer & Humi 2001). Here the blast wave momentum $P = \sqrt{\Gamma^2-1}$, $M_0 = E_0/\Gamma_0$ is the initial baryon loading, that is, the baryonic mass mixed into the explosion, and $m(x)$ is the swept-up mass (all masses are now in energy units). The internal energy, excluding rest mass energy, is given by

$$U' = U'(x) = m_p\int_0^\infty dp'(\gamma'_p-1)N'(p';x) = 4\pi m_p\int_0^x dx_i\; x_i^2\; n_0(x_i)\;(\bar\gamma-1)\;, \tag{31}$$

where $p' = \sqrt{\gamma_p'^2-1}$ is the proton's dimensionless momentum in the comoving frame, γ'_p its Lorentz factor, and

$$\bar p = \bar p(x,x_i) = \sqrt{\bar\gamma^2-1} = P(x_i)\;\left(\frac{x_i}{x}\right)\;\left[\frac{\Gamma(x)}{\Gamma(x_i)}\right]^{1/3} \tag{32}$$

solves the equation for momentum evolution of a nonthermal proton in a blast wave with thickness $\Delta' = f_\Delta x/\Gamma$ (Panaitescu & Mészáros 1999; Dermer & Humi 2001). Here only adiabatic losses are considered for the protons, and f_Δ is assumed to remain constant with x and take the value 1/12. The differential swept-up mass

$$\frac{dm(x)}{dx} = 4\pi m_p x^2\; n_0(x)\;, \tag{33}$$

where $n_0(x)$ is the circumburst medium density, assumed to be radially symmetric about the GRB source. The internal energy U' changes due to volume expansion and adiabatic losses according to the relation

$$\frac{dU'_{adi}}{dx} = -\;\frac{4\pi m_p}{x}\;(1-\frac{1}{3}\frac{d\ln\Gamma}{d\ln x})\;\int_0^x dx_i\; x_i^2\; n_0(x_i)(\frac{\bar p^2}{\bar\gamma})\;. \tag{34}$$

We consider two case scenarios to simulate the change in internal energy due to a photohadronic discharge:

1. A fraction ξ of the internal energy is instantaneously radiated away at $x = x_0$. Following the discharge, the blast wave is again assumed to sweep up circumburst material and evolve adiabatically. In this case, $U'(x)$ and dU'_{adi}/dx are given by eqs. (31) and (34), respectively, at $x \le x_0$. At $x > x_0$,

$$\frac{U'(x)}{4\pi m_p} = (1-\xi)\int_0^{x_0} dx_i\; x_i^2\; n_0(x_i)\;(\bar\gamma-1) + \int_{x_0}^x dx_i\; x_i^2\; n_0(x_i)\;(\bar\gamma-1)\;, \tag{35}$$

and

$$-\frac{dU'_{adi}}{dx} = \frac{4\pi m_p}{x}\;(1-\frac{1}{3}\frac{d\ln\Gamma}{d\ln x})\;\times \Big[(1-\xi)\;\int_0^{x_0} dx_i\; x_i^2\; n_0(x_i)(\frac{\bar p^2}{\bar\gamma}) + \int_{x_0}^x dx_i\; x_i^2\; n_0(x_i)(\frac{\bar p^2}{\bar\gamma})\;\Big]. \tag{36}$$

2. The internal energy is radiated on an exponential dissipation timescale t'_{int}, followed by a recovery of the blast wave to adiabatic behavior at $x \ge x_0$. Thus

$$\frac{U'(x)}{4\pi m_p} = \int_0^x dx_i\; x_i^2 n_0(x_i)(\bar\gamma-1)\exp[-t'(x_i)/t'_{int}] + H(x-x_0)\int_{x_0}^x dx_i\; x_i^2\; n_0(x_i)\;(\bar\gamma-1)\,, \tag{37}$$

and

$$-\frac{dU'_{adi}}{dx} = \frac{4\pi m_p}{x}\;(1-\frac{1}{3}\frac{d\ln\Gamma}{d\ln x})\;\times \Big[\int_0^x dx_i\; x_i^2\; n_0(x_i)(\frac{\bar p^2}{\bar\gamma})\exp[-t'(x_i)/t'_{int}] + H(x-x_0)\int_{x_0}^x dx_i\; x_i^2\; n_0(x_i)(\frac{\bar p^2}{\bar\gamma})\Big]\;, \tag{38}$$

for all $x > 0$.

We consider first Case 1 with Parameter Set 1,[2] with a sudden loss of radiative energy taking place at $x_0 = 5\times10^{16}$ cm, corresponding to an observer time of $\approx$ 650 s after the start of the GRB—essentially the same timescale when photopion losses and escape become important (Fig. 2b). In Fig. 4(a), the numerical solutions to the equations for the evolution of P are plotted for $\xi = 0, 0.5, 0.9, 0.99$. Also shown are some approximations to the dynamics of the blast wave when $\xi = 0$ (see Dermer & Humi 2001); the curve labeled "momentum conservation solution" has the term dU'_{adi}/dx set equal to zero; the curve labeled "analytic blast wave" is eq. (4); the curve labeled "momentum conservation solution" shows the analytic form for a fully radiative blast wave (Blandford & McKee 1976; Chiang & Dermer 1999). The inset gives P as a function of observer time using the numerical solution to eqs. (30), (35), and (38), for different values of ζ.

Fig. 4b shows the terms $P\Gamma(dm/dx)$ and $-(P + P^{-1})(dU'/dx)_{adi}$ in the numerator of eq. (30) for Parameter Set 1 with $\xi = 0, 0.5, 0.9$, and 0.99, and Fig.

[2] The microphysical parameters are irrelevant in this treatment of blastwave dynamics, though this may not be true in general, particularly for radiative GRBs with $\epsilon_{B-1} > 1$ in the fast cooling regime.

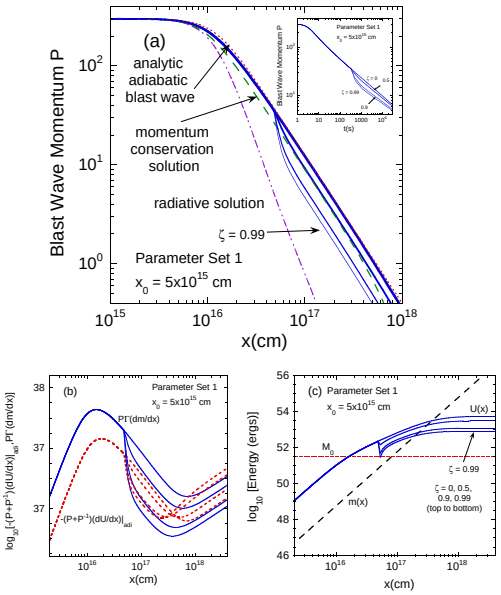

FIG. 4.— (a) Solid curves show the evolution of a GRB blast wave as a function of x for different fractional discharges $\xi = 0, 0.5, 0.9,$ and 0.99, for Parameter Set 1. Also shown are approximations to the case with $\xi = 0$ (see text). Inset shows blastwave evolution as a function of observer time. (b) Variation of values of the terms in the numerator of eq. (30), as labeled. (c) Variation of values of the terms in the denominator of eq. (30), as labeled.

4c shows the terms M_0, $m(x)$ and $U'(x)$ in the denominator of eq. (30). A reasonable approximation to blastwave dynamics can be obtained, when the blast wave is relativistic, by neglecting the $(dU'/dx)_{adi}$ term because this term is a small, constant fraction of the sweep-up term $P\Gamma(dm/dx)$. When the blast wave becomes non-relativistic, at $x \cong 4 \times 10^{17}$ cm for these parameters, the $(dU'/dx)_{adi}$ term must be retained. In Fig. 4c, the range of x where the M_0, $U'(x)$ amd $m(x)$ terms dominate the value of the denominator of eq. (30) define the coasting, relativistic self-similar, and non-relativistic self-similar regimes, respectively. In the Case 1 scenario, after the instantaneous discharge at x_0, the blast wave rapidly decelerates, but then recovers its adiabatic behavior as it sweeps up additional material from the circumburst medium.

An instantaneous discharge may be oversimplified, however, because a discharge of any sort must take place over a finite time exceeding at least $\Delta r'/c$, the light travel timescale across the blastwave width. For this reason we now consider the Case 2 Scenario, again with Parameter Set 1. Here the blastwave is assumed to recover its adiabatic behavior at $x_0 = 5 \times 10^{16}$ cm after suffering an exponential discharge with comoving (exponential-)loss timescales $t'_{esc} = 10$, 20, 40, and 80 ks. Although this is sufficient to solve the blastwave dynamics, at least in the limit $\epsilon_{e-1} \lesssim 1$, it still is not clear what is the shape of the light curve.

We can derive some *idealized light curves* by weighting internal energies and rates by the beaming factor Γ^2 that boosts energy and rate in a spherical blastwave. The following weightings are employed, keeping in mind that this sort of approach neglects particle cooling and spectral effects. The weightings considered are

1. $\Gamma^2 U'$, so that the comoving power is assumed to be proportional to the total internal energy, as might correspond to a single species emitter that radiates in the adiabatic limit;

2. $\Gamma^2 L'$, where the comoving power L' is set equal to the swept-up power $4\pi x^2 n_0 m_p c^3 \beta(\Gamma^2 - \Gamma)$, so this case would represent the bolometric leptonic luminosity of a GRB radiating in the strong cooling regime;

3. $\Gamma^2 U'^2$, so that the comoving power is proportional to the square of the internal energy, as might hold in a scenario involving wave-particle coupling; and

4. $\Gamma^2 U'^2/(x/x_d)^3$, where the comoving power is assumed proportional to the product of the total internal energy and energy density, for example, of the magnetic field.

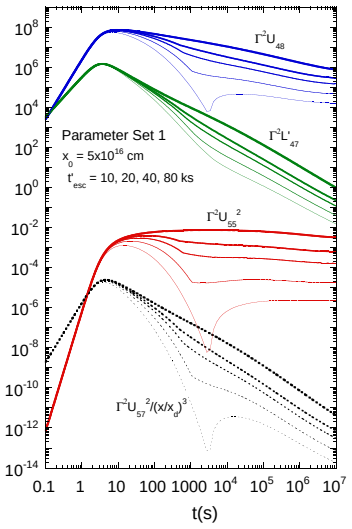

FIG. 5.— Idealized light curves for the Case 2, Parameter Set 1 Scenario with $x_0 = 5 \times 10^{16}$ cm and $t'_{esc} = 10$, 20, 40, and 80 ks.

Fig. 5 shows some numerical solutions for the Case 2, Parameter Set 1 Scenario with the different weightings just described. The blast wave is assumed to recover its adiabatic character at $x_0/x_d \cong 4.2$. The notation here is that $U' = 10^{\#} U'_{\#}$ ergs and $L' = 10^{\#} L'_{\#}$ ergs s^{-1}. Overlooking the shape of the light curves at early times—a point to which we return soon—these synthetic light curves resemble the Swift BAT/XRT X-ray light curves of GRBs. On top of these generic light curve shapes are the X-ray flares made by some as yet unspecified mechanism.

The various weightings reflect different underlying assumptions of the physical model and yield a variety of temporal behaviors that could explain the range of X-ray light curves observed with Swift. The sensitivity of the model light curves to the location x_0 where the blast wave begins to evolve adiabatically and the comoving discharge timescales is illustrated in Fig. 6, showing model light curves with a range of X-ray declines and plateau-like features.

5. DISCUSSION

The central idea proposed here is that the rapid X-ray declines and plateaus discovered in $\sim$ keV light curves of GRBs by the Swift team (Barthelmy et al.

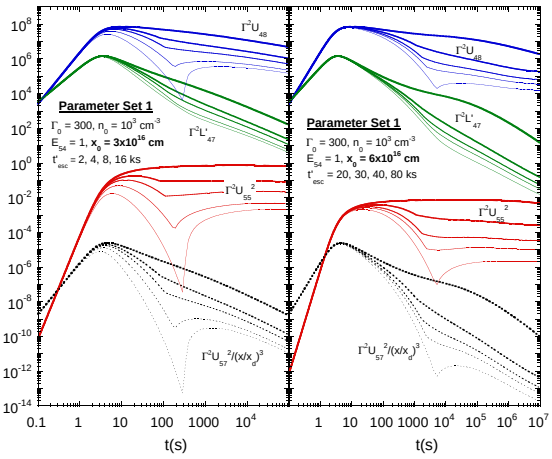

FIG. 6.— Idealized light curves for the Case 2, Parameter Set 1 Scenario with (a) $x_0 = 3 \times 10^{16}$ cm and $t'_{esc} = 2$, 4, 8, and 16 ks, and (b) $x_0 = 6 \times 10^{16}$ cm and $t'_{esc} = 20$, 30, 40, and 80 ks.

2005; Tagliaferri et al. 2005; O'Brien et al. 2006) are signatures of UHECR acceleration in GRBs. The solution to the problem of UHECR origin may involve a variety of source classes, but must involve at least one source class, and GRBs offer a very attractive solution: They are found outside our Galaxy (and possibly in our Galaxy; see Wick et al. (2004); Melott et al. (2004); Dermer & Holmes (2005)), which must be the case to make UHECRs with Larmor radii larger than can be contained in the Milky Way; they are energetic, with each explosion releasing as much as $\sim 10^{52}$ ergs kinetic energy (Friedman & Bloom 2005; Le & Dermer 2007), much of it in very clean, highly relativistic bulk particle or field-dominated outflows; and they are impulsive, at least on recurrence times $\gtrsim$ day. This last is important by leading to a prediction of no clustering or angular correlations on the sky of UHECRs originating from GRBs (Waxman & Miralda-Escude 1996).

Simple (pre-BeppoSAX) BATSE estimates for the required local emissivity in super-GZK ($\gtrsim 10^{20}$ eV) UHECRs compared with the emissivity in X-rays and γ rays from GRBs, assumed to be at a mean redshift $\langle z \rangle \approx 1$, agree to within $\sim$ 1 order of magnitude, suggesting a connection between the two (Waxman 1995; Vietri 1995; Dermer 2002). If GRBs are the progenitors of UHECRs, then the superposed cosmic-ray intensity spectrum from all the UHECR GRB sources over cosmic time display features of propagation. Most pronounced are the GZK feature and the ankle feature, the latter of which is likely due to pair production (Berezinskii & Grigor'eva 1988; Wick et al. 2004; Berezinsky et al. 2005). If Auger measures a spectrum similar to the HighRes spectrum at energies $\gtrsim 10^{19.5}$ eV, then these spectral features of cosmic rays, accumulated during transport from the source to the detector, are reasonably well-explained within a scenario where UHECRs originate from cosmic rays, with clearcut predictions for GZK neutrino fluxes.

Here we extend the scenario that UHECRs originate from GRBs by entertaining the hypothesis that the X-ray light curves of GRBs show a spectral feature associated with UHECR acceleration. The synthetic bolometric light curves in Figs. 5 and 6 are idealized, but contain the basic features of more realistic calculations that depend on a wide range of underlying assumptions about particle acceleration and the fraction of energy going into magnetic fields and waves. Depending on the radiation model, the internal and external shock contribution, and the setting of the zero of time, a wide range of X-ray decays can be understood within this picture.

An important feature of this scenario is that a large fraction of the swept-up internal energy resides in protons accelerated to ultra-high energies. Photopion processes effectively discharge the particle energy in the form of a neutral beam (Atoyan & Dermer 2003; Dermer & Atoyan 2004). The decay of the internal particle energy density weakens the magnetic field through feedback of the particle energy into field energy, halting further acceleration while hastening escape of the remaining UHECRs found in the blast wave, until a dominant fraction, $\gtrsim 90\%$ (depending on the initial amount of energy contained in the nonthermal protons), is lost from the blast wave as a neutral beam.

Developing detailed physical models to simulate leptonic and hadronic acceleration and loss is beyond the scope of a single paper, but the various physics issues that enter into a combined leptonic/hadronic GRB model can be described in somewhat more detail. We break the discussion into a consideration of

1. the acceleration mechanism;
2. light curves in an internal/external shock scenario;
3. light curves in an external shock scenario;
4. explanation for the rapid X-ray declines;
5. explanation for the plateau phase; and
6. predictions of this scenario.

5.1. *Acceleration*

Acceleration to super-GZK energies is possible via stochastic processes in the blast-wave shell (Dermer & Humi 2001) and through acceleration by the internal shocks in a colliding shell model (e.g., Waxman 1995). Acceleration to such energies through shock Fermi processes is not possible through relativistic external shocks formed in a surrounding medium with magnetic field $\sim \mu$G (Gallant and Achterberg 1999), but might be possible if the GRB takes place in a highly magnetized environment, as might be expected if the surroundings are formed by the stellar winds of high-mass stars (e.g., Völk and Biermann 1988, noting limitations imposed by total energy contained in the magnetized wind), or if the upstream field is amplified by streaming cosmic rays, for example, by the Bell & Lucek (2001) mechanism (O'C. Drury et al. 2003).

Here, acceleration of swept-up protons to ultra-high energies is assumed to take place by second-order gyroresonant processes in the blast wave shell. This is reflected in the derivation of the acceleration rate, eq. (23), which contains only shocked fluid quantities. A turbulent, stochastic Type 2 Fermi mechanism in the blast-wave shell formed by a relativistic (internal or external) shock can make a highly efficient accelerator (Dermer & Humi 2001), which is a sort of turbulent boiler discussed decades ago (Ochelkov & Prilutskii 1975, and references therein), though here found in

the shocked fluid shell of a relativistic blast wave. The basic coupling involves gyroresonant acceleration of ions and electrons interacting with MHD wave turbulence (in the context of Solar flares, see, e.g., Steinacker and Miller 1992; Miller and Ramaty 1989; Miller and Roberts 1995), the form of which is model-dependent and may furthermore involve anisotropic coupling depending on wave type (Goldreich 2001). But for isotropic power-law wave turbulence, acceleration through the stochastic Fermi mechanism makes hard number spectra ($n(\gamma) \propto \gamma^{-s}$), with $s \approx 1$ and most of the energy content consequently in the highest particle energies (Schlickeiser 1984, 1989; Dermer et al. 1996; Dermer & Humi 2001). Combined first- and second-order processes (e.g., Schlickeiser 1984; Krülls 1992; Ostrowski & Schlickeiser 1993) suggest that steeper spectra, with $1.5 \lesssim s \lesssim 2$, would be formed in this sort of scenario. But if $s \lesssim 2$, most of the energy resides in the highest energy particles, which can be accelerated to energies $\gtrsim 10^{20}$ eV (Dermer 2006).

The gyroresonant wave-particle interactions accelerate particles dynamically, so no steady state is reached (analytic solutions to time-dependent particle evolution through second-order processes are given by, e.g., Park & Petrosian 1995; Becker, Le, & Dermer 2006), and energy flows between waves, particles, and fields until it is discharged from the system. The bulk kinetic energy of the blast wave, initially dissipated in the shell as highly nonthermal internal particle kinetic energy as well as field and wave energy, is transformed into a component of ultra-relativistic protons carrying a large fraction of the total energy. This internal energy, including the wave energy that continues to be fed into the particles, is discharged when photopion losses become sufficiently great. Growth of the target photon field, for example, from proton synchrotron and photohadronic secondaries followed by electromagnetic cascading, can lead to an photohadronic or proton-synchrotron loop instability of the type considered by Kirk & Mastichiadis (1992) to extract increasingly more energy of the UHECRs until the internal energy content is effective discharged. Obviously, more model studies are required to quantify the total fraction of internal energy that can be discharged in this way.

Under the given circumstances, $\sim 10^{18}$ eV photopion neutrinos are created from the decay of photomeson secondaries, ultra-high energy neutrons escape if they avoid further photopion interactions, and an electromagnetic channel consisting of γ rays and e^+ and e^- initiates a cascade, ultimately leading to a flux of escaping γ rays (Atoyan & Dermer 2003). The cosmic-ray neutron discharge from GRB blast waves, as considered here, produces a component of the UHECRs, causing the ionic composition of UHECRs to be proton-dominated. The decaying UHE neutrons and, indeed, photoprocesses by the highest energy protons and ions make an UHE synchrotron decay halo (Dermer 2002; Ioka et al. 2004) around host galaxies. The mean injection spectrum per GRB by this process has not been calculated from first principles, but could range from a flat $\gamma^2\dot{n}(\gamma)$ over a narrow energy range $\sim 10^{19}$ – 10^{21} eV, as in the model of Waxman & Bahcall (1999), to a power-law injection $\gamma^2\dot{n}(\gamma) \propto \gamma^{-0.2}$, as in the model by Wick et al. (2004). In principle, this process could also operate in radio/γ-loud AGNs, and produce spectra as steep as $\gamma^2\dot{n}(\gamma) \propto \gamma^{-0.7}$ found in the models of Berezinsky et al. (2006).

The acceleration mechanism in a colliding shell scenario is much different than stochastic acceleration in the fluid shell, but the photohadronic discharge mechanism could certainly operate in such a system, though the details still need to be worked out. Incidentally, the potential importance of second-order processes in GRB blast waves may negate the concerns of Ghisellini et al. (2000) that the GRB must display a strong-cooling spectrum. Second-order acceleration competing with leptonic radiative and adiabatic energy losses can form a low-energy pileup in the electron distribution, so that no cooling tail appears. Indeed, the shape of broadband time-averaged spectra of GRBs (Schaefer et al. 1998), interpreted as nonthermal leptonic synchrotron radiation, seems to require an abrupt low-energy cutoff and may be consistent with an electron pileup at some lower energy due to combined first- and second-order processes with cooling. This question will take greater urgency when GLAST provides combined GLAST GBM, GLAST LAT, and Swift BAT and XRT GRB light curves, permitting detailed spectral analysis of bright GRBs from the prompt to afterglow phases. This will reveal the transition from the internal shocks (in the internal/external shock scenario) to external shocks, as now considered.

5.2. *Internal/External Model*

In the internal/external scenario (Piran 1999, 2005; Mészáros 2006), the transition from the prompt phase formed by colliding shells of jet plasma to the afterglow phase made by external shocks takes place no later than the time of BeppoSAX reorientation, ~ 8 hrs, and likely much sooner. In this picture, the internal shocks make a distinct radiation signature from the external shock emission received later. The zero of time for the external shock emissions from the GRB can, in the internal/external scenario, be set to various times, but is determined observationally when the GRB detector is triggered, e.g., by precursor emission. In the case of a GRB exploding in a uniform circumburst medium, the latest the zero of time can be set would be about when the external shock signature reaches its maximum brightness and triggers the GRB detector, which is generally near the deceleration time t_d. The freedom to set the zero of time (Lazzati & Begelman 2006; Kobayashi & Zhang 2007) when modeling data with the external shock component considered here, as shown in Fig. 7, adds an additional distortion and increased variety to the model light curves, similar to various behaviors of the X-ray light curves found with Swift.

An alternate view of the internal/external model is to have all the prompt emissions up to the time of the rapid X-ray declines made by internal shock processes (see §5.5). Here it is surprising that the Swift BAT light curves are rather smooth and apparently not a superposition of generic kinematic curvature light pulses (Yamazaki et al. 2006; Dermer 2004), although the last pulse in some GRBs, for example, Swift XRT data of GRB 061202 ~ 120 s after burst trigger (GCN Report 19 2006), do appear possibly to represent the last major accretion events from a hypothetical collapsar torus. In either variant of the internal/external scenario, a complete model GRB light curve would combine the model

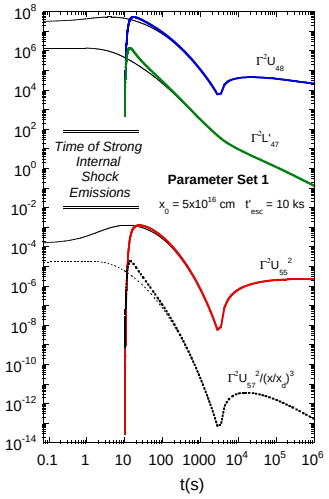

FIG. 7.— Idealized light curves for the Case 2, Parameter Set 1 Scenario with $x_0 = 5 \times 10^{16}$ cm and $t'_{esc} = 10$ ks, with the time reset to -3 s and + 10 s for the thin and thick curves, respectively.

light curves calculated in an external shock treatment with a second component consisting of γ-ray pulses and X-ray flares from colliding shells made by central engine activity.

Placing these calculations in the context of the internal/external approach, the transition from internal shock to external shock emissions takes place, typically, between 50 and 100 seconds, precisely in the gap between BAT and XRT, at which time the flux levels of the internal and external shock components are roughly equal. It may seem coincidental that the times for the transitions from internal to external shocks are $\approx t_d$ (cf. Zhang et al. 2006). Swift observations of late-time X-ray flares interpreted as central engine activity mean, however, that the internal shocks operate over a wide range of times, nullifying to some extent this coincidence. It may also appear coincidental that the flux level of the rising external-shock component is at about the same level as the earlier prompt internal shock component. But the large fraction ($\gtrsim$ 90%) of swept-up energy in the form of nonthermal hadrons, the factor 10 – 100 more nonthermal energy in the shells before the radiative discharge compared to after, and the low efficiency $\sim$ 1 – 10% for transforming internal shock energy to hard X-rays and γ rays (Beloborodov 2000; Kumar 1999; Guetta, Piran, & Waxman 2004), naturally leads to the expectation that energy radiated in afterglow phase is comparable to that of the prompt phase, so that the similar flux levels of the internal and external shock components may not be so surprising.

We conclude that the proposed interpretation for the fast decays is in accord with the internal/external shock scenario for GRBs, provided that the external shock emissions make a significant contribution already in the early afterglow.

5.3. *External Shock Model*

A conceptually simpler though not generally accepted approach is to suppose that all GRB emissions are formed by a single impulsive event. In such a picture, the γ-ray pulses and X-ray flares seen in GRB light curves are a consequence of interactions of the blast wave with a clumpy circumburst density (Dermer & Mitman 1999, 2004), and there is a single blast wave that is energized only by the external forward/reverse shock pair.

The central requirement for short timescale variability in this model is that the size scale of the inhomogeneities (clouds) is $\ll x/\Gamma_0$ (Dermer & Mitman 1999), and that the blast wave remains thin in order to form a strong forward shock, which translates into the condition that the blast wave spreading is $\lesssim x/\Gamma_0^3$ (Dermer 2006, 2007). Even late-time X-ray flares could be the result of a GRB blast wave intercepting clumps of material if the blast-wave shell remains thin (Dermer 2007). A prediction of this model is that ranges of baryon loading, in particular, mass-loaded dirty fireballs (Dermer et al. 1999), can account for the differences between classical long duration GRBs and X-ray flashes.

This model has been questioned on ground of efficiency (Sari & Piran 1997; Piran 2005), but the argument is incorrect (Dermer & Mitman 2004). The additional energy content in the prompt phase makes high efficiency for the external shock model, as for the internal shell model, less critical, improving the viability of both models. Another concern is that late sharp flaring events cannot be made by external shocks. The simulation of Zhang et al. (2006) treats however a large cloud, and the treatment of Nakar & Granot (2006) operates in the adiabatic self-similar phase, after which much of the blast-wave energy has already been converted to radiation (this mistake, and the failure to take into account beaming factors for the interaction, is also made by Ioka et al. 2005). The brightest flares are made by portions of the blast wave that have not yet entered this phase, and which intercept a dense clump of material with a thick column (Dermer & Mitman 1999). See Dermer (2007) for a fuller discussion.

Whether or not a "pure" external shock model for GRBs can be defended, the proposed model is already in accord with the internal/external scenario, as already described. It is also interesting to note that McMahon et al. (2004) find that the afterglow ϵ_B parameter must be much weaker than in the prompt phase to explain light curves of certain smoothly varying GRB.

5.4. *Explanation for the Rapid Decay*

We have considered a physical mechanism to explain the rapid decays observed with Swift from GRBs in the late prompt/early afterglow phase that could operate in both internal/external and external shock scenarios. The number of physical models for this effect is not yet large; there is a preference recently (e.g., Nava et al. 2007; Panaitescu 2006; O'Brien et al. 2006a; Zhang et al. 2006; Liang et al. 2006) to quantify the effect and perform empirical phenomenological studies rather than to construct physical models. An exception is Pe'er et al. (2006), who consider scattering of GRB emission in a cocoon formed as the blast wave jet emerges from the stellar photosphere (see also Pe'er et al. 2006a). The emergent photons can exhibit a steep temporal decay, similar to the GRB X-ray light curves observed with Swift XRT. This model applies strictly to a collapsar scenario, where the shocks emerge from the stellar photosphere by forming a cocoon (e.g., Ramirez-Ruiz et al. 2002), yet rapid decays also occur in short, hard GRBs (e.g., GRB 050724, Barthelmy et al. 2005a), which are thought to originate from coalescence events that lack stellar photospheres

and cocoons (for recent reviews of short hard GRBs, see Nakar 2007; Lee & Ramirez-Ruiz 2007).[3]

The curvature effect (Kumar & Panaitescu 2000; Dermer 2004; Liang et al. 2006), which limits the rate at which an impulsively illuminated shell can temporally decay, obviously plays an important role. The curvature limits apply to the case of an active central engine that suddenly shuts itself off, or dramatically reduces its activity, as in the model of Proga & Zhang (2006). For a spherical blast wave that is roughly uniform within the Doppler cone, the curvature limits would also apply to internal or external shocks. The model presented here is in accord with the curvature limit, keeping in mind the uncertainty in setting the zero of time (see also Lazzati & Begelman 2006).

From a comparison of the idealized bolometric light curves in Figs. 5 –8 with the Swift BAT and XRT GRB light curves shown in, e.g., the O'Brien et al. (2006) paper, it seems that the model offers adequate variety to explain the rapid X-ray decays, and not simply an average light curve (O'Brien et al. 2006a).

5.5. *Explanation for the Plateau Phase*

Focusing on the external shock component in the proposed scenario, about the time that Fermi processes can accelerate a large fraction of the particle energy to ultra-high energies, photohadronic losses and escape become important and cause a sudden loss of internal energy. The magnetic field energy, which is supported by the internal energy, itself becomes smaller, thereby enhancing nonthermal particle escape and causing the internal energy to collapse. At some point, the energy content in the blast wave reaches its minimum when only the original baryon load and a remnant magnetic field remains. Magnetic field generation processes like the Weibel instability (e.g., Nishikawa et al. 2006) could then amplify the blast wave magnetic field until plasma is swept-up and entrained, and the blast wave again commences to evolve adiabatically.

The viability of this explanation for the plateau phase and the diversity of X-ray light curves discovered by Swift (Barthelmy et al. 2005) is suggested by the wide range of idealized light curve profiles calculated and plotted in Figs. 5 – 7, though more research will be required to quantify the underlying assumptions about the acceleration and particle radiation mechanisms that will allow fits to data. This explanation is quite different from the conventional explanation in the internal/external scenario. There, delayed energy injection (e.g., Zhang & Mészáros 2001; Zhang et al. 2006), possibly signaled by the late-time X-ray flares, could harden the temporal decay. Yet plateau phases are often seen soon after a rapid decay, as in the cases cited in the Introduction, so the central engine activity has to be concealed while powering the light curve. An analysis of GRB 050713A by Guetta et al. (2007) starts with the conclusion that the behavior of GRB 050713A requires refreshed shocks. Toma et al. (2006) consider a patchy jet scenario where the delayed off-axis emissions become brighter than the on-axis emissions, but their model lacks a self-Compton component, and the afterglow X-ray component lasts much longer than found in detailed numerical calculations with similar parameters (Dermer et al. 2000). Fan & Piran (2006) try to model this behavior and assess the energy requirements. They claim that powering the hard afterglow phase does not make excessive demands on energetics, but do not display blast-wave solutions characteristic of the rapid decay and plateau phases discovered (Nousek et al. 2006; Zhang et al. 2006) with Swift.

[3] This invites the speculation that the short hard class of GRBs are also sources of UHECRs, given appropriate parameters, in particular, small variability times.

5.6. *Predictions*

Besides the steep decays and plateau phases in the X-ray light curves from GRBs, there are other direct radiative signatures for the hypothesis that UHECRs originate from GRBs. In all cases where photopion losses are important, the blast wave is assumed to be radiating in the fast-cooling limit, so that the νF_ν indices $a \cong 1/2$ and $b = 1 - (s/2)$, where s is the electron injection index (with $s \approx 2.2$ for shock Fermi models). If we accept that accelerated electrons radiatively cool without being subsequently accelerated (contrary, incidentally, to the point made earlier with respect to the concerns of Ghisellini et al. (2000)), then already a careful spectral analysis for the variation of ϵ_{pk} predicted by external shock emissions as it sweeps through the Swift XRT detector could see if GRB blast waves evolve within a few hundred seconds to a condition where the ϵ_e and ϵ_B parameters are each $\gtrsim 10\%$.

A prediction of this model is hadronic γ-ray light consisting of proton synchrotron, photopion and secondary photohadronic decay radiations that cascade to low enough energies that internal and diffuse cosmic $\gamma\gamma$ attenuation processes become negligible. This component varies differently from the X-ray lepton synchrotron component and can appear much after the prompt emissions. The hadronic emission component could then possibly account for the delayed γ-ray emission in GRB 940217 (Hurley et al. 1994) and GRB 941017 (González et al. 2003), likely in addition to SSC emission. The independently varying hadronic emission component is a prediction for GLAST, though a leptonic model (e.g., Pe'er & Waxman 2004) for delayed anomalous components that includes Compton-scattered forward- and reverse-shock emissions, could also make a delayed component as observed from GRB 941017.

Ultra-high energy neutrinos are made by the release of blast wave energy though this mechanism, and we predict the detection of a delayed neutrino flux at high energies just about the time of the rapid decays. Unfortunately, the $\gtrsim 10^{17}$ eV neutrinos from the photohadronic processes in GRB blast waves are at a difficult energy for IceCube to detect, but the $\gtrsim 10^{18}$ eV neutrinos could be detected in sideways showers with Auger, or in balloon-borne detectors such as ANITA. Besides the UHE neutrino component, PeV neutrinos detectable with IceCube will be made during the prompt phase in the internal shell/collapsar model in large fluence GRBs when the shocked shell Lorentz factors ~ 100 – 200, while being optically thick to $\gamma\gamma$ attenuation at GeV energies (Dermer & Atoyan 2003; Razzaque et al. 2004; Guetta et al. 2004).

For parameters that make a highly radiative blast wave phase, $\epsilon_{p,syn}$ for proton synchrotron emissions from UHECRs in GRBs will be found in the TeV range. To

avoid attenuation by the diffuse intergalactic infrared radiation fields, this emission could only be detected from low redshift, $z \lesssim 0.4$, GRBs, which can be measured with low-threshold air Cherenkov telescopes such as MAGIC. The photon flux at these energies is very low, so only a few $\gtrsim 100$ GeV photons could be detected with a direct photon detection telescope such as GLAST.

6. SUMMARY AND CONCLUSIONS

By carrying through an analysis of a complete leptonic/hadronic GRB blast-wave model, a region of parameter space was found for GRB external shocks where, even in the simplest constant density blastwave model, photohadronic processes have important effects on blastwave evolution. This occurs for the observer a few hundred seconds after the start of the GRB for circumburst medium densities $n_0 \gtrsim 10^2$ cm^{-3}, $100 \lesssim \Gamma_0 \lesssim 300$, $E_{54} \sim 1 - 10$, and $\epsilon_e, \epsilon_B \gtrsim 10\%$. For these parameters, the time scales for photopion losses and direct escape become comparable to the available time in the early afterglow, with observable consequences.

The GRB blast wave is predicted to evolve toward the strong cooling regime in the early afterglow, leading to a strong discharge of energy through photohadronic processes and direct escape of UHECR ions, causing the declines in the X-ray light curves observed by Swift. The change of ϵ_{pk} with time may indicate the evolution of the radiative regime during the prompt and early afterglow phases, though this component can be concealed in an internal/external shock model by internal shock emissions. Hadronic radiations consisting of high-energy neutrinos, cascade γ rays, and escaping cosmic-ray neutrons could be important to $\gtrsim 10^4$ s after the GRB, producing a component that varies, in general, differently from the X-ray lepton sychrotron emission. As a prediction for GLAST, this component should be bright at GeV energies just before the times that the rapid X-ray declines are observed. A related flux of $\gtrsim 10^{17}$ eV neutrinos is made at this time.

The release of energy in the form of neutrons or escaping ions in the early afterglow phase means that there was much more energy in the GRB blast wave during the prompt phase. Thus the efficiency of γ-ray production during the prompt phase is low, which ameliorates efficiency concerns in both external or internal shock models. Hadronic processes imprint GRB light curves and the UHECR spectrum with distinctive signatures. The rapid X-ray declines and plateau phases discovered with Swift are argued here to be just such signatures.

I thank A. Atoyan, M. Böttcher, and J. Chiang for collaboration and comments, and Dr. E. Nakar for pointing out how this solution could resolve efficiency concerns in GRB models. I also sincerely thank the referee for a thorough and constructive report. This work is supported by the Office of Naval Research, by NASA *GLAST* Science Investigation No. DPR-S-1563-Y, and NASA Swift Guest Investigator Grant No. DPR-NNG05ED41I.

REFERENCES

Atoyan, A. M., & Dermer, C. D. 2003, ApJ, 586, 79
Barthelmy, S. D. et al. 2005, ApJ, 635, L133
Barthelmy, S. D. et al. 2005a, Nature, 438, 994
Becker, P. A., Le, T., & Dermer, C. D. 2006, ApJ, 647, 539
Bell, A. R., & Lucek, S. G. 2001, MNRAS, 321, 433
Beloborodov, A. M. 2000, ApJ, 539, L25
Berezinskii, V. S., & Grigor'eva, S. I. 1988, A&A, 199, 1
Berezinsky, V., Gazizov, A. Z., & Grigorieva, S. I. 2005, Physics Letters B, 612, 147
Berezinsky, V., Gazizov, A., & Grigorieva, S. 2006, Phys. Rev. D, 74, 043005
Blandford, R. D., & McKee, C. F. 1976, Physics of Fluids, 19, 1130
Böttcher, M., & Dermer, C. D. 1998, ApJ, 499, L131
Böttcher, M., & Dermer, C. D. 2000, ApJ, 532, 281
Chiang, J., & Dermer, C. D. 1999, ApJ, 512, 699
Dermer, C. D., Chiang, J., Böttcher, M. 1999, ApJ, 513, 656
Dermer, C. D. 2002, ApJ, 574, 65
Dermer, C. D. 2004, ApJ, 614, 284
Dermer, C. D. 2007, submitted to astro-ph/0702—
Dermer, C. D. 2006, Venice Swift Workshop, astro-ph/0611194
Dermer, C. D., Miller, J. A., and Li, H. 1996, ApJ, 456, 106
Dermer, C. D., Chiang, J., & Mitman, K. E. 2000, ApJ, 537, 785
Dermer, C. D., & Atoyan, A. 2003, Physical Review Letters, 91, 071102
Dermer, C. D., & Atoyan, A. 2004, Astron. Astrophys., 418, L5
Dermer, C. D., & Holmes, M. 2005, ApJ, 628, L21
Dermer, C. D., & Humi, M. 2001, ApJ, 556, 479
Dermer, C. D., & Mitman, K. E. 1999, ApJ, 513, L5
Dermer, C. D., & Mitman, K. E. 2004, Astronomical Society of the Pacific Conference Series, 312, 301
O'C. Drury, L., van der Swaluw, E., & Carroll, O. 2003, ArXiv Astrophysics e-prints, arXiv:astro-ph/0309820
Fan, Y., & Piran, T. 2006, MNRAS, 369, 197
Friedman, A. S., & Bloom, J. S. 2005, ApJ, 627, 1
Gallant, Y. A., and Achterberg, A., 1999, MNRAS, 305, L6
GCN Report 19.1. http://gcn.gsfc.nasa.gov/reports/report_19_1.pdf
Gehrels, N., et al. 2004, ApJ, 611, 1005
González, M. M., Dingus, B. L., Kaneko, Y., Preece, R. D., Dermer, C. D., & Briggs, M. S. 2003, Nature, 424, 749
Ghisellini, G., Celotti, A., & Lazzati, D. 2000, MNRAS, 313, L1
Goldreich, P. 2001, Ap&SS, 278, 17
Guetta, D., Hooper, D., Alvarez-Muñiz, J., Halzen, F., & Reuveni, E. 2004, Astroparticle Physics, 20, 429
Guetta, D., Piran, T., & Waxman, E. 2005, Astrophys. J., 619, 412
Guetta, D., et al. 2007, A&A, 461, 95
Hillas, A. M. 1984, ARA&A, 22, 425
Hurley, K. 1994, Nature, 372, 652
Ioka, K., Kobayashi, S., & Mészáros, P. 2004, ApJ, 613, L17
Ioka, K., Kobayashi, S., & Zhang, B. 2005, ApJ, 631, 429
Kirk, J. G., & Mastichiadis, A. 1992, Nature, 360, 135
Kobayashi, S., & Zhang, B. 2007, ApJ, 655, 973
Krülls, M. F. 1992, A&A, 260, 49F
Kumar, P. 1999, ApJ, 523, L113
Kumar, P., & Panaitescu, A. 2000, ApJ, 541, L51
Lazzati, D., & Begelman, M. C. 2006, ApJ, 641, 972
Lee, W. H., & Ramirez-Ruiz, E. 2007, New Journal of Physics (astro-ph/0701874)
Le, T., & Dermer, C. D. 2007, ApJ, in press (astro-ph/0610043)
Liang, E. W., et al. 2006, ApJ, 646, 351
Liu, S., Melia, F., & Petrosian, V. 2006, ApJ, 636, 798
McMahon, E., Kumar, P., & Panaitescu, A. 2004, MNRAS, 354, 915
Melott, A. L., et al. 2004, Internat. J. Astrobiology, 3. 55
Mészáros, P. 2006, Reports of Progress in Physics, 69, 2259
Mészáros, P., & Rees, M. J. 1993, ApJ, 405, 278
Miller, J. A., and Roberts, D. A. 1995, ApJ, 452, 912
Miller, J. A., and Ramaty, R. 1989, ApJ, 344, 973
Nava, L., Ghisellini, G., Ghirlanda, G., Cabrera, J. I., Firmani, C., & Avila-Reese, V. 2007, ArXiv Astrophysics e-prints, arXiv:astro-ph/0701705
Nakar, E., & Granot, J. 2006, astro-ph/0606011
Nakar, E. 2007, Physics Reports, in press (astro-ph/0701748)
Nishikawa, K.-I., Hardee, P. E., Hededal, C. B., & Fishman, G. J. 2006, ApJ, 642, 1267
Nousek, J. A., et al. 2006, ApJ, 642, 389
O'Brien, P. T., et al., 2006, ApJ, 647, 1213
O'Brien, P. T., Willingale, R., Osborne, J. P., & Goad, M. R. 2006a, New Journal of Physics, 8, 121

Ochelkov, I. P., & Prilutskii, O. F. 1975, Soviet Astronomy, 18, 708
Ostrowski, M. O. & Schlickeiser, R. 1993, A&A, 268, 812
Panaitescu, A. 2006, ArXiv Astrophysics e-prints, arXiv:astro-ph/0607396
Panaitescu, A., & Mészáros, P. 1999, ApJ, 526, 707
Park, B. T., & Petrosian, V. 1995, ApJ, 446, 699
Pe'er, A., Mészáros, P., & Rees, M. J. 2006, ApJ, 652, 482
Pe'er, A., Mészáros, P., & Rees, M. J. 2006, ApJ, 642, 995
Pe'er, A., & Waxman, E. 2004, ApJ, 603, L1
Proga, D., & Zhang, B. 2006, MNRAS, 370, L61
Piran, T. 1999, Phys. Reports, 314, 575
Piran, T. 2005, Reviews of Modern Physics, 76, 1143
Rachen, J. P., & Mészáros, P. 1998, Phys. Rev. D, 58, 123005
Ramirez-Ruiz, E., Celotti, A., & Rees, M. J. 2002, MNRAS, 337, 1349
Razzaque, S., Mészáros, P., & Zhang, B. 2004, ApJ, 613, 1072
Sari, R., Piran, T., & Narayan, R. 1998, ApJ, 497, L17
Sari, R., & Piran, T. 1997, ApJ, 485, 270
Schaefer, B. E., et al. 1998, ApJ, 492, 696
Schlickeiser, R. 1984, A&A, 136, 227
Schlickeiser, R. 1989, Astrophys. J., 336, 243
Steinacker, J., and Miller, J. A. 1992, Astrophys. J., 393, 764
Tagliaferri, G., et al., 2005, Nature, 436, 985
Toma, K., Ioka, K., Yamazaki, R., & Nakamura, T. 2006, ApJ, 640, L139
Vietri, M. 1995, ApJ, 453, 883
Vietri, M. 1998, ApJ, 507, 40
Völk, H. J. and Biermann, P. L. 1988, ApJ, 333, L65
Waxman, E. 1995, Physical Review Letters, 75, 386
Waxman, E., & Bahcall, J. 1999, Phys. Rev. D, 59, 023002
Waxman, E., & Miralda-Escude, J. 1996, ApJ, 472, L89
Wick, S. D., Dermer, C. D., & Atoyan, A. 2004, Astroparticle Physics, 21, 125
Willingale, R., et al. 2006, ApJ, submitted (astro-ph/0612031)
Yamazaki, R., Toma, K., Ioka, K., & Nakamura, T. 2006, MNRAS, 369, 311
Zhang, B., & Mészáros, P. 2001, ApJ, 552, L35
Zhang, B., Fan, Y. Z., Dyks, J., Kobayashi, S., Mészáros, P., Burrows, D. N., Nousek, J. A., & Gehrels, N. 2006, ApJ, 642, 354
Zhang, B.-B., Liang, E.-W., & Zhang, B. 2006, astro-ph/0612246